Oscillator Microfabrication, Micromagnets, and Magnetic Resonance Force Microscopy

Jae-Hyuk Choi,[a] Utkur M. Mirsaidov,[a] Casey W. Miller,[a] Yong J. Lee,[a] Samaresh Guchhait,[a] Michelle D. Chabot,[b] Wei Lu,[a] and John T. Markert[a]

[a]Department of Physics C1600, University of Texas, Austin, TX 78712, USA;
[b]Department of Physics, University of San Diego, San Diego, CA 92110, USA

ABSTRACT

We report our advances in nuclear magnetic resonance force microscopy (NMRFM) in three areas: 1) MEMS microfabrication studies of single-crystal-silicon mechanical oscillators using double-sided processing; 2) micromagnetometry, anisotropy, and dissipation studies of individual permalloy micromagnets on oscillators; and 3) mechanical-oscillator detection of NMR in the magnet-on-oscillator scanning mode. In the first area, we report details of our back-etch microfabrication process, and characterize oscillator resonant frequency, quality factor, and spring constant by measuring the noise spectral density of oscillator motion. In the second studies, we report changes in the resonant frequency and quality factor for each of four modes of our oscillators for two shapes and sizes of permalloy thin-film (∼30 and 180 nm) micromagnets; a simple, quantitative model is used to describe both low-field softening and high-field stiffening. Finally, we report scanning-mode NMR force detection of an ammonium-sulfate single-crystal interface and a polymethyl-methyl-acrylate thin film at room temperature. These latter studies use 2-μm-radius permalloy magnets on silicon oscillators to image the NMR response from resonant volumes as small as 3 μm^3. These NMRFM studies are the first reported that attain sub-micron resonant-slice resolution at room temperature.

Keywords: Mechanical Oscillator, Microfabrication, Micromagnets, Magnetic Resonance Force Microscopy

1. INTRODUCTION

The field of nuclear magnetic resonance force microscopy (NMRFM)[1] has potential for nanometer-scale NMR detection and three-dimensional imaging; future applications may include molecular imaging, subsurface defect detection, and direct manipulation of single spins and controlled entanglement of nearby spins for quantum computing. Instead of the inductive detection used in conventional NMR, the NMRFM technique couples the magnetic moment $\mathbf{M}$ of the precessing nuclei to the field gradient ∇B of a micromagnet. Our experimental arrangement is shown in Fig. 1. The micromagnet is mounted on an ultra-sensitive mechanical micro-oscillator, and the resulting force $\mathbf{F} = (\mathbf{M} \cdot \nabla)\mathbf{B}$ is measured by detecting the oscillator motion, typically using fiber-optic interferometry. To our knowledge, the work presented here is the first report of room-temperature sub-micron NMRFM detection. These experiments represent progress in oscillator fabrication, controlled design of magnet-on-oscillator properties, and ultra-small force detection. We describe our recent progress in the fabrication of our sensitive multi-mode micro-oscillators in Section 2. In Section 3, we present the results of systematic studies of micromagnets on oscillators in an external magnetic field; the field dependence of the resonant frequency and quality factor are described for each of the four major oscillation modes (the symmetric and antisymmetric modes of both cantilever and torsional motion). Our earlier, initial demonstrations of the NMRFM technique used a simple sample-on-oscillator configuration.[2] In Section 4, we report our first results of NMRFM detection in the magnet-on-oscillator configuration, the technique most useful for high-sensitivity scanning-mode implementation of NMRFM.

Further author information: (Send correspondence to J.T.M.)
J.T.M.: E-mail: markert@physics.utexas.edu
C.W.M: current address: Department of Physics 0354, University of California, San Diego, La Jolla, CA 92093, USA.

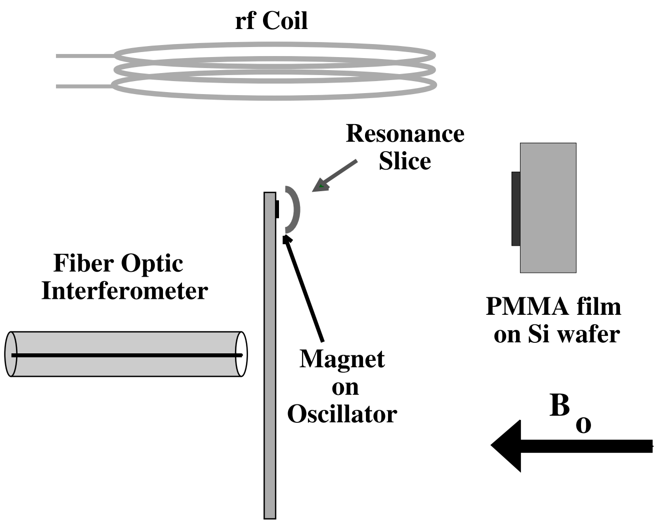

Figure 1. The NMRFM experiment. The nuclear spins in the PMMA film are cyclically inverted at the mechanical oscillator frequency by the rf field. As the PMMA sample is brought closer to the oscillator, an ac magnetic force is detected when the resonant slice coincides with the sample position.

2. OSCILLATOR FABRICATION

We have found that our double-torsional oscillator design[3] (see the first panel of Fig. 2) offers attractive advantages: comparable force sensitivity to other ultrasensitive mechanical oscillators in a thicker, thus more robust, structure. We further discuss the various oscillation modes and review their advantages below. Our recent progress on these oscillators centers on a much different fabrication process than previously implemented. Many previous oscillator designs of ours[2,3] and others[4] utilize one-sided processing to etch around and release the oscillator structures. However, we anticipate that ultimate improvements in oscillator quality factor Q will require fabrication techniques that protect the final single-crystal structures from undue etch-induced deterioration.

We have thus implemented a double-sided processing technique for the fabrication of our double-torsional oscillators. The main aim is to protect as much as possible the boron-implanted single-crystal regions that will become the oscillator structures; the addition of back-etch processing preserves the structures until the last, brief etch step. The process flow is shown in Fig. 2. The fabrication starts with a silicon (100) wafer, which is implanted with boron on one side. After rapid thermal annealing (RTA) in order to rebuild the single-crystal structure, the oscillator pattern is transferred to a photoresist (PR) layer using optical lithography. The photoresist left after developing serves as a masking layer for a HBr reactive ion etch (RIE). The RIE serves to etch the oscillator patterns into the wafer by etching away the boron implanted silicon layer that has no front-side pattern. Then we deposit a thin (~ 150 nm) layer of low temperature oxide (LTO) to both sides of wafer. The backside is then patterned to provide etch windows for the oscillators. An infrared aligner is used to coordinate the backside mask with respect to the front side pattern. We selectively etch through the wafer thickness only at these windows, so that the rest of the wafer can provide structural support during the final etch or handling. We have used TMAH (tetramethyl ammonium hydroxide) solution for wet etchant as well as KOH (potassium hydroxide). When KOH is used, Si_3N_4 was deposited instead of LTO. After the backside lithography, and when the back etch is almost complete, another reactive ion etch run is carried out to etch through the masking LTO (or Si_3N_4) layer. Then the oscillator wafer was put back in the etch solution for the complete release. The oscillators are rinsed thoroughly with distilled water before being dried. We have freeze-dried and used different liquids such as acetone, isopropanol, or methanol in order to decrease the level of stiction due to the surface tension of the liquid.

We have successfully used the double-torsional design[5] previously for small force detection[6,7] and discussed its use for NMRFM.[2,3] The main motivation for this design is the improved Q made possible in the antisymmetric

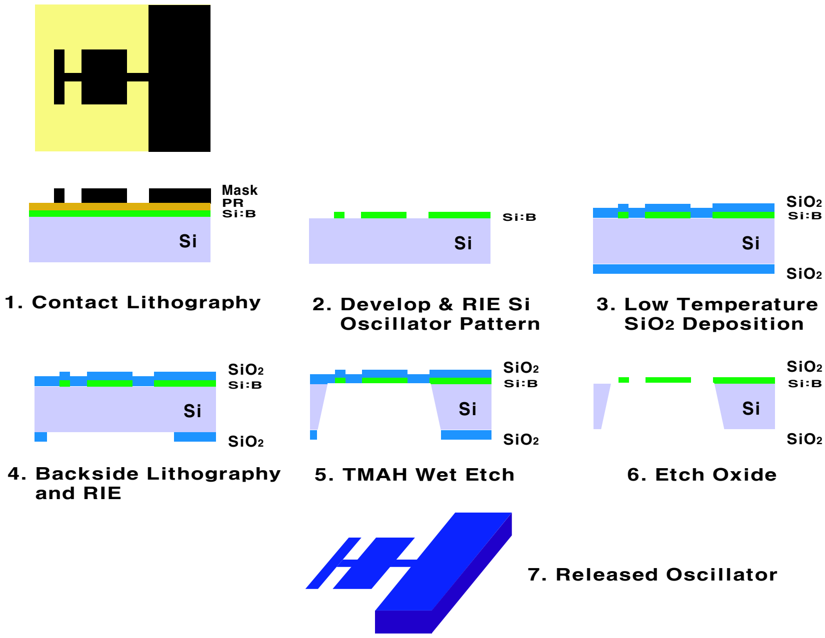

Figure 2. Process flow for two-sided processing of double-torsional oscillators.

torsional mode: with a smaller moment on top (the "head"), the motion of the lower segment (the "wings") is so small that there is very little residual dissipation transmitted through the base. The current oscillator chip holds five oscillators with the different ratio of moments of inertia of the "wing" to that of the "head": 2, 4, 6, 12, and 32. An oscillator with a moment ratio of 4 is shown in Fig. 3. Initially we have investigated the mechanical resonance parameters of the oscillator with the inertia ratio of 6 as a function of temperature. In order to facilitate the search of the resonance frequencies of normal modes, we also have carried out finite element analysis modeling using the commercial software *Ansys*. The modal analysis quite accurately located the normal mode frequencies of the fabricated oscillator. The following table contains the simulation results as well as experimental measurements at room temperature for a 1.0-μm thick, 200-μm tall double-torsional oscillator, with 15 μm-wide necks (293 K).

Table 1. Simulated and measured normal mode frequencies for 1.0-μm thick mechanical oscillators.

Mode	*Ansys* simulation	Experimental measurement
Symmetric cantilever	19.2 kHz	18.3 kHz
Symmetric torsional	68.4 kHz	62.9 kHz
Antisymmetric cantilever	123 kHz	125 kHz
Antisymmetric torsional	205 kHz	208 kHz

Because the boron-implanted oscillators were well protected during processing, these regions were much thicker (1.0 μm) than the thickness typically obtained from front-etch processes (0.3 μm). We have initially investigated the lower cantilever resonance (the simple bending mode) due to the large signal obtainable through-

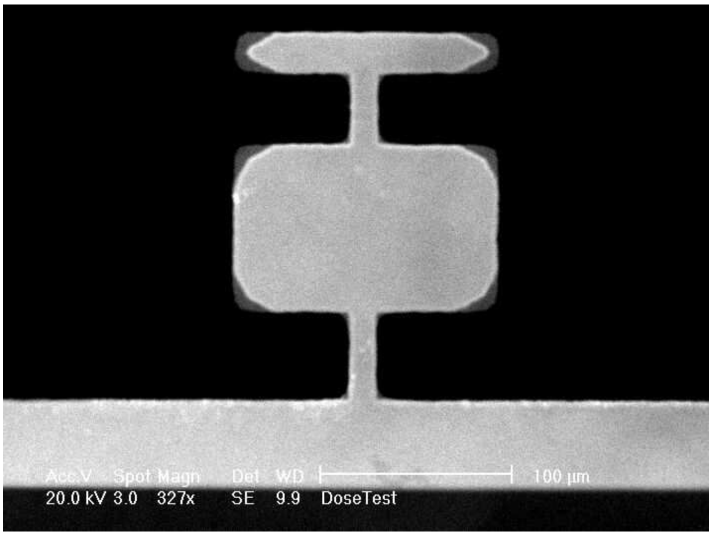

Figure 3. A double-torsional oscillator fabricated with the back-etch process of Fig. 2.

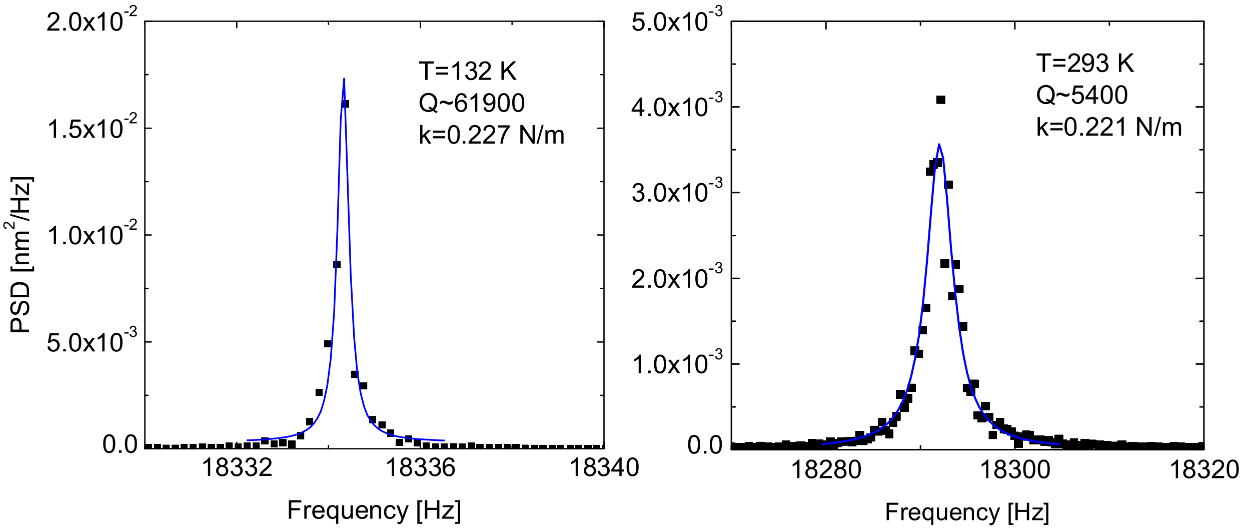

Figure 4. Noise power spectral density of a back-etch-processed single-crystal silicon mechanical oscillator at two temperatures for the symmetric cantilever mode, obtained by Fourier transform of time-dependent thermal noise amplitude fluctuations. The values of f_o and Q extracted from this data are in agreement with driven frequency sweeps, and since the form of the thermal noise force is known, these data also provide values of the spring constant k_s.

out the temperature range; also, since this recent batch of oscillators was relatively thick (1.0 μm), the resonant frequencies were high, and only this mode well satisfies the adiabatic requirement of NMRFM: under typical conditions, the manipulated sample paramagnetism must be cyclically inverted at frequencies less than about 50 kHz. Resonance parameters were obtained through piezoelectrically-driven frequency scans as well as through measurement of the spectral density of motion fluctuations (thermal noise).

For the noise measurement, the root mean square amplitude is related to the temperature through the equipartition theorem: $k_s < x^2 > = k_B T$, where k_s is the spring constant, k_B is Boltzmann's constant, and T is temperature. We have measured the RMS vibration of the thermal-noise-driven oscillator at several temperatures. Typical data are shown in Fig. 4. The location and shape of the spectra give the resonant frequency and Q of

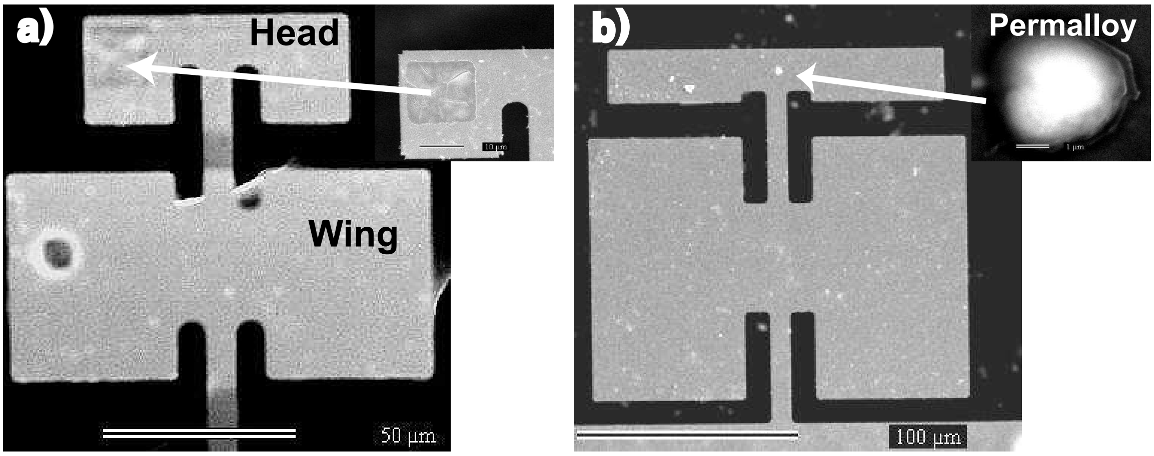

Figure 5. Double-torsional micro-oscillators used in the micromagnetometry experiments. Oscillator A, on the left, has a larger magnet (15×15 $\mu\mathrm{m}^2$) and normal modes at 24.9, 53.2, 135, and 161 kHz. Oscillator B on the right has the smaller magnet (3 μm diameter) and normal modes at 5.6, 9.9, 29.6, and 49.9 kHz.

the oscillator directly; using the equipartition theorem, the interferometry-calibrated noise amplitude gives the experimentally measured spring constant of ~ 0.22 N/m for these thick oscillators. As the temperature decreases below room temperature, some increase in Q was observed (Fig. 4). We will report full temperature-dependent data elsewhere, once we have fully analyzed possible laser-induced heating[8, 9] and self-oscillation phenomena, including thermally-driven and direct-momentum-transfer effects.

3. PROPERTIES OF MAGNETS ON OSCILLATORS

In order to study the effects of mounting micromagnets on mechanical oscillator properties, we have extended our prior thin-film micromagnetometry measurements[10] to much smaller magnets. In addition to quantitative measurements of the magnetic moment and magnetic anisotropy of our micromagnets, we determined both the effect of oscillating the magnets in an external magnetic field on oscillator Q. Such determinations are required to properly model the behavior of our micromagnets during NMRFM experiments.

For these studies we used an earlier generation of single-crystal silicon double-torsional oscillators (Fig. 5); these had a thickness of $\sim$500 nm and other design considerations (note the long oscillator necks in Fig. 5) to maintain low resonant frequencies for NMRFM. Oscillators with two different magnets will be discussed; Oscillator A has a 15 μm $\times$ 15 μm, 30-nm-thick and Oscillator B has a 3 μm-diameter, 180-nm-thick Permalloy ($Ni_{80}Fe_{20}$) magnet. Although several other oscillation modes[3] were observed, we limited this study to only the four major oscillation modes discussed above: the lower (symmetric) and upper (antisymmetric) cantilever and torsional modes, as shown in Fig. 6.

To determine the resonant frequencies, the oscillators were glued with GE7031 varnish to a piezoelectric plate that was shaken by an applied sinusoidal voltage. The resulting motion of the oscillator was detected by a fiber optic interferometer; the zero-field resonant frequencies detected are given in the caption of Fig. 5. Phase sensitive detection on the right and the left sides of the head and wing was used to identify the resonant modes of the oscillator. These measurements were carried out at room temperature and 10^{-5} torr. To investigate the field dependence of the resonant modes, driven frequency scans were performed for several values of an external magnetic field that was applied perpendicularly to the plane of the oscillator (and thus the Permalloy film); this is the geometry appropriate for the NMRFM experiments described below. The field-dependent resonant frequencies and quality factors were obtained from fits of a Lorentzian to the driven scans. Our experimental results are shown in Fig. 7. The frequency shift is normalized to the zero-field resonance of each mode. As previously observed, the oscillators exhibit two regimes of field dependence: there is an initial softening at low fields, followed by a stiffening at high fields. Increasing the external field causes the magnetic moment of the film

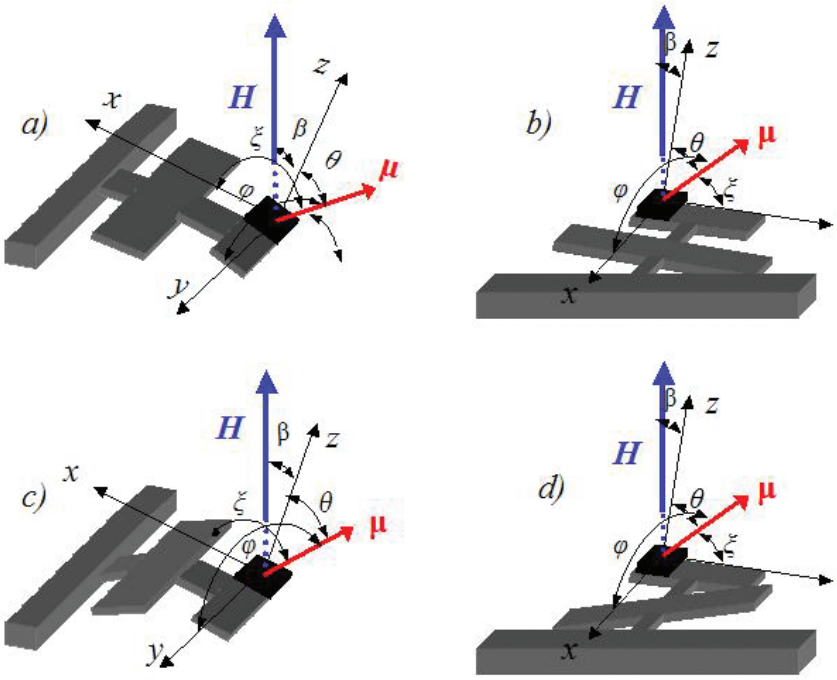

Figure 6. The major oscillation modes of our double-torsional oscillators, and the geometry used to determine the magnetic energy and equilibrium moment direction. a) The lower cantilever mode. b) The lower torsional mode. c) The upper cantilever mode. d) The upper torsional mode.

to rotate from its initial in-plane orientation, due to shape anisotropy, through intermediate orientations, and ultimately into alignment with the field at high field values. Resonant frequencies of the lower and the upper cantilever modes decrease (softening regime) for fields less than a switching field of about 1 T, then increase (stiffening regime) for higher fields. The switching field for the lower and upper torsional modes was found to be about 0.6 T. The resonant frequencies of the upper torsional and cantilever modes exhibit smaller relative field-induced changes than the lower modes; this is because the comparable magnetic torques have a smaller absolute effect at higher frequencies.

The field dependence of the resonant frequencies of the four oscillator modes can be understood within a single-domain model of the magnet on the oscillator. The model parameters and geometry we use are given in Fig. 6, above. We first consider the cantilever modes, and then apply a similar formulation for the torsional modes. Due to shape anisotropy, the easy plane of the magnet is in the plane of the oscillator. The energy functional (up to a constant) for this case can be written as:

$$\frac{E}{V} = K_x \sin^2 \xi + K_y \sin^2 \phi - M_s H (\cos\beta \cos\theta - \sin\beta \cos\phi)\,, \tag{1}$$

where K_x and K_y are first-order anisotropy constants in x and y directions, respectively, and M_s is the saturation magnetization. The energy of the system can be minimized with respect to ϕ and θ to find the direction of the magnetic moment of the domain. Using trigonometric identities to rearrange the Hamiltonian and assuming that the oscillator deflection angle $\beta \ll 1$, we obtain

$$\cos\theta = \frac{H}{H_{k,x}} \qquad \text{and} \qquad \cos\phi = \frac{H}{H_{k,yx}}\beta \tag{2}$$

where $H_{k,x} = 2K_x/M_s$ and $H_{k,yx} = 2(K_y - K_x)/M_s$. The x component of the magnetic torque is

$$\tau_x = \mu_y H_z - \mu_z H_y = -\mu H^2 \beta \left(\frac{1}{H_{k,x}} - \frac{1}{H_{k,yx}} \right) . \tag{3}$$

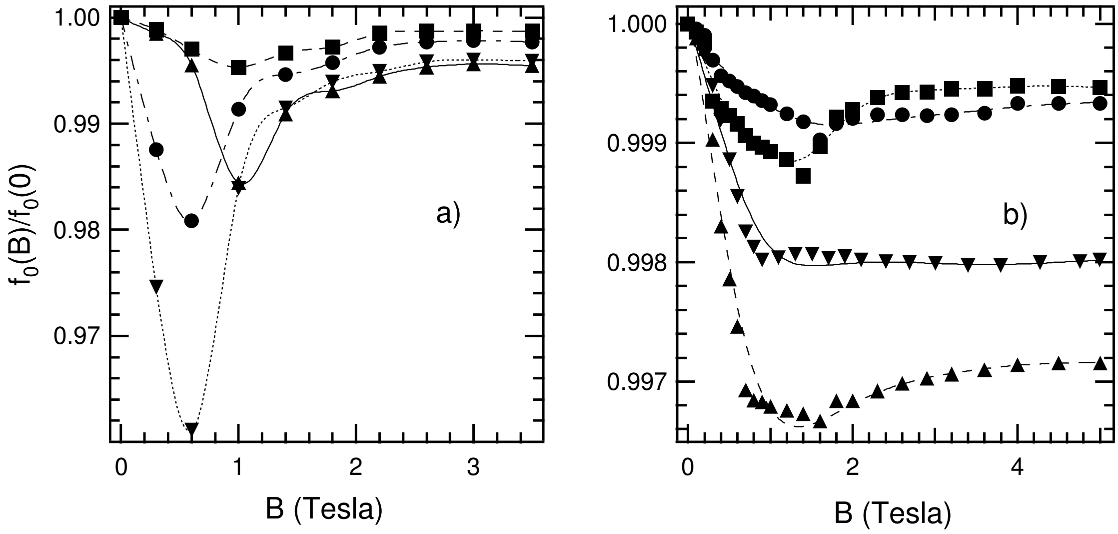

Figure 7. Magnetic-field-dependent resonant frequencies relative to the zero-field value for Oscillator A (large magnet, left panel) and Oscillator B (small magnet, right panel). In each case the modes are: lower cantilever (upward triangles), lower torsional (downward triangles), upper cantilever (squares), and upper torsional (circles).

We equate this with the restoring torque, $\tau_x = \Delta k_o/\beta L_{eff}$ to obtain the frequency shifts $\Delta f_o/f_o = \frac{1}{2}\Delta k_o/k_o$. Here, Δk_o is the spring constant change and L_{eff} is the effective length of the cantilever. For fields H below $H_{k,x}$ this gives

$$\frac{\Delta f_o}{f_o} = -\frac{\mu H^2}{2k_o L_{eff}^2}\left(\frac{1}{H_{k,x}} - \frac{1}{H_{k,yx}}\right). \tag{4}$$

At high enough fields, when $H > H_{k,x}$, the magnetic moment approaches the y-z plane. This results in the special case $\xi = \pi/2$ and $\sin\phi = -\cos\theta$. Our energy then takes form $E/V = K_y \sin^2\phi - M_s H - H\cos(\beta - \phi)$, yielding a magnetic torque[11] of the form $\tau_x = \mu H \beta[H_{k,x}/(H + H_{k,x})]$. From this we obtain (for $H > H_{k,x}$)

$$\frac{\Delta f_o}{f_o} = \frac{\mu H}{2k_o L_{eff}^2}\frac{H_{k,x}}{(H + H_{k,x})}. \tag{5}$$

Equations (4) and (5) describe softening and stiffening behavior of the oscillator. Our model suggests that both the lower and upper cantilever modes have the same transition field between these two regimes.

For the torsional modes the same reasoning applies, but we must instead consider the restoring torque about the y axis, $\tau_y = \Delta\kappa_o\beta$, where $\Delta\kappa_o$ is the change in torsion constant. The resulting frequency shifts are identical in form to Eqs. (4) and (5), with $H_{k,y} = 2K_y/M_s$, $H_{k,xy} = 2(K_x - K_y)/M_s$, and the torsion constant κ_o substituted for $H_{k,x}$, $H_{k,yx}$, and the product $k_o L_{eff}^2$, respectively. Thus we also see that both the lower and upper torsional modes have same transition field, and this field is different from that of the cantilever modes.

Since the relative frequency shift of a cantilever (torsional) mode is inversely proportional to the spring (torsional) constant, such shifts are smaller for the higher frequency modes, as is evident in Fig. 7. For our oscillators with parameters $L_{eff} \approx 100$–150 μm, $k_s \approx 0.01$–0.030 N/m, and $\kappa_o \approx 6.0 \times 10^{-10}$ N·m, the fits to Eqs. (4) and (5) are shown in Fig. 8. The fits provide a moment measurement for the larger magnet of Oscillator A of $\mu = 4.6 \times 10^{-12}$J/T, in agreement with the value $\mu = 4.5 \times 10^{-12}$ J/T from the volume and the permalloy saturation magnetization value of 670 kA/m. For the smaller magnet of Oscillator B, the extracted moment is 8.3×10^{-13} J/T, in fair agreement with the value 1.1×10^{-12} J/T, calculated with appreciable volume uncertainty. The extracted anisotropy fields for the larger magnet are $H_{k,x} = -0.83$ T and $H_{k,y} = -0.80$ T; these are nearly equal, as expected from the nearly square shape; for the smaller magnet, the values are $H_{k,x} = -0.60$ T and $H_{k,y} = -0.87$ T, reflecting the more irregular shape of the smaller magnet.

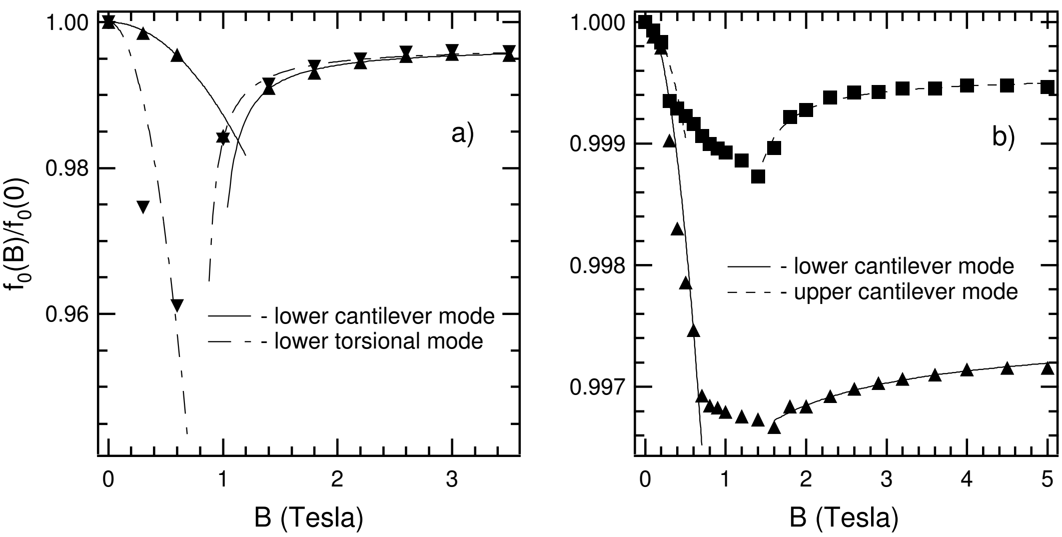

Figure 8. Fits to the low-field and high-field regimes of the field-dependent mechanical oscillator resonant frequency, using Eqs. (4) and (5).

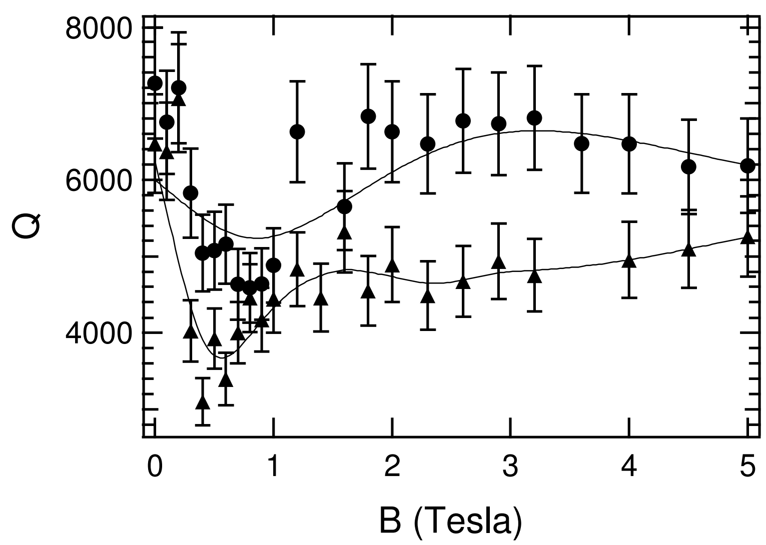

Figure 9. Quality factor as a function of field for the lower cantilever mode of Oscillator A (triangles) and Oscillator B (circles). Lines are guides to the eye.

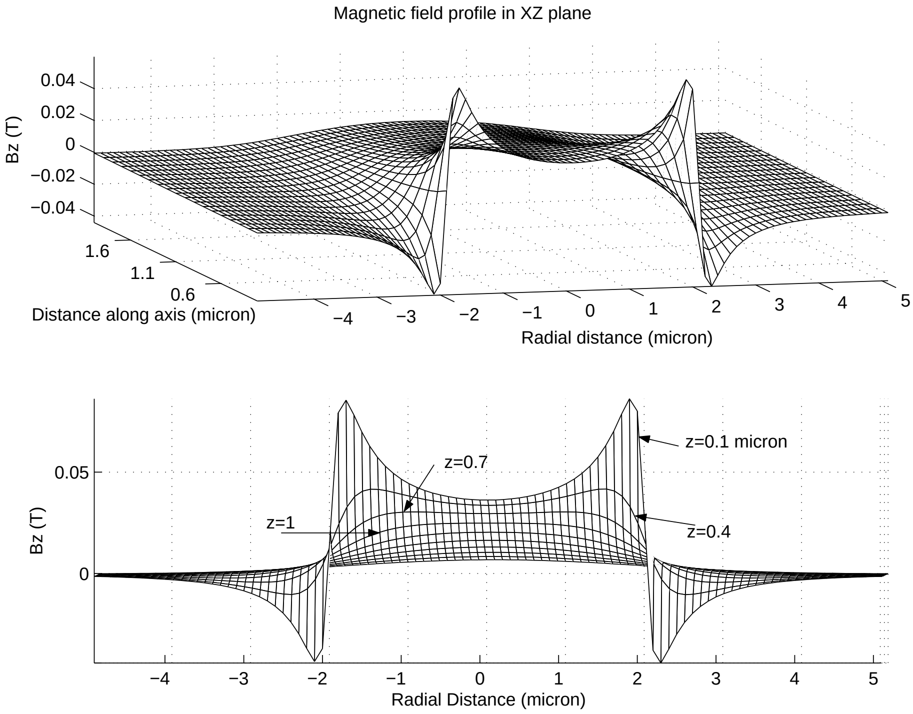

Figure 10. Upper frame: The magnetic field (vertical axis) in tesla as a function of distance in a plane through the axis of the disk-shaped micromagnet used for NMRFM. Lower frame: The projection of the data of the upper frame on the micromagnet plane, showing the shape of resonant slices for different distances from the micromagnet.

The quality factors for the lower cantilever and upper torsional modes are shown in Fig. 9. The quality factor tends to decrease at low fields as the moment tilts out of the plane, and then recovers to nearly the zero-field value for fields much higher than the anisotropy fields. Thus, in addition to obtaining a direct determination of the value of our micromagnet moment, we also determine anisotropy and fluctuation information. The implications for NMRFM are good: at the high fields ($\sim$8 T) of our NMRFM experiments, the moment of the micromagnet is saturated out of plane (parallel to the applied field), the oscillator frequency becomes nearly independent of field, and the oscillator Q is not appreciably decreased from its zero-field value.

4. NUCLEAR MAGNETIC RESONANCE FORCE MICROSCOPY EXPERIMENTS

The experimental arrangement for our NMRFM experiments was shown in Fig. 1. Two experiments are described here. First, we mention a scan near the surface of a large ($\sim$1 mm^3) single crystal of ammonium sulfate, $(NH_4)_2SO_4$. This scan was optimized to obtain the smallest resonant slice thickness of our experiments to date, $\leq$ 200 nm. Second, in preparation for future three-dimensional studies of structure and dynamics in polymer films, we report initial one-dimensional scan measurements on a 0.3-μm thin film of PMMA (polymethyl-methyl-acrylate), a common photoresist. We now describe some general experimental details and magnetic modeling before examining the data.

For both experiments, an external magnetic field $B_o = 8.1$ T was used. With the additional inhomogeneous micromagnet field, NMRFM experiments were performed near 8.2 T, at rf frequencies in the range 343–345 MHz. The applied rf field amplitude was approximately 1.0 mT. In order to match the frequency of the sample moment variations with the mechanical oscillator frequency, the rf field was frequency modulated at the oscillator frequency, providing cyclic inversions of the sample moment;[12] the amplitude of the frequency modulation was

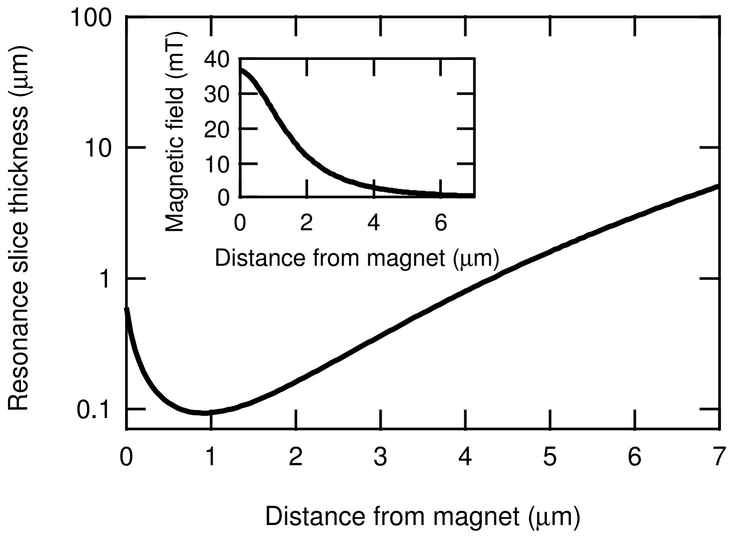

Figure 11. The resonant slice thickness as a function of distance from the micromagnet. Inset: the field contribution of the micromagnet vs. distance.

$\Omega = 31.2$ kHz. The mechanical oscillators used here had spring constants near $k_s = 2.0 \times 10^{-4}$ N/m, resonant frequencies of 3.9–4.0 kHz, and Q values in the range 1–6$\times 10^3$.

The size of the slice of the sample's nuclear paramagnetism to be detected is a function of the shape of our Permalloy thin film magnet. For these experiments, the magnets fabricated had diameters of 4.0 μm and thickness of 180 nm. Figure 10 shows the field distribution near such a disk-shaped micromagnet, which acts much like a ring of current. The lower frame shows a projection of the field contours at different distances from the magnet. It is evident that near a distance $z = 1.0\,\mu$m, fairly flat resonant slices, with lateral dimension of radius 2.0 μm and varying thickness can be obtained. The resonant slice thickness is given by $\Delta z = 2\Omega/\gamma\nabla B$ and is plotted in Fig. 11. As is evident, resonant slice thicknesses as low as $\sim$100 nm can be attained close to these magnets.

In the first experiment, the ammonium sulfate crystal acts essentially as an infinitely thick slab. The sample is very suitable, both due to its long spin-lattice relaxation time $T_1 \approx 5$ s and large proton spin density $n_H = 6.5 \times 10^{22}$ cm^{-3}. The crystals are easily cleaved to yield a flat vacuum-sample interface. Figure 12 shows a one-dimensional scan of the oscillator ring-up signal as a function of the resonant slice position. A smooth background signal, due to induced oscillator motion from the frequency-modulated rf signal, has been subtracted from the data (see below). The force noise is at the level of the expected thermal noise, $F_{\rm noise} = 2.5 \times 10^{-16}$ N. The measured amplitude corresponds to a force signal of approximately $F_{\rm expt} = 9.7 \times 10^{-16}$ N, in fair agreement with our estimate from the sample's Curie nuclear paramagentism and resonant slice volume, $F_{\rm predicted} = 7.6 \times 10^{-16}$ N. Most noticeably, the flat geometry gives a sharp onset to the NMR force signal. Although the resonant slice may be as thin as 100 nm, we estimate, due to curvature in the field contours, misalignment, and our data steps, that our resolution is closer to 200 nm.

Next, a one-dimensional scan of the PMMA thin film was performed. The raw data is shown in the inset of Fig. 13, where the background (artifact) signal can be seen to have a smooth variation, inversely proportional to the distance between the sample and the resonant slice position. The NMRFM signal (solid curve) appears at the expected location, 1.0 μm from the oscillator (for these measurements, the sample was brought in contact with the oscillator, and then retracted to the desired distance). A force of about 2.0×10^{-15} N is detected, with a signal to noise of about 4. The dotted curve shows similar data with the sample 2.0 μm from the oscillator; as expected from the smaller field gradient there, the signal strength decreases to about one-half of the value of the first scan. These data are promising for the future scanning-mode microscopy of polymer structures.

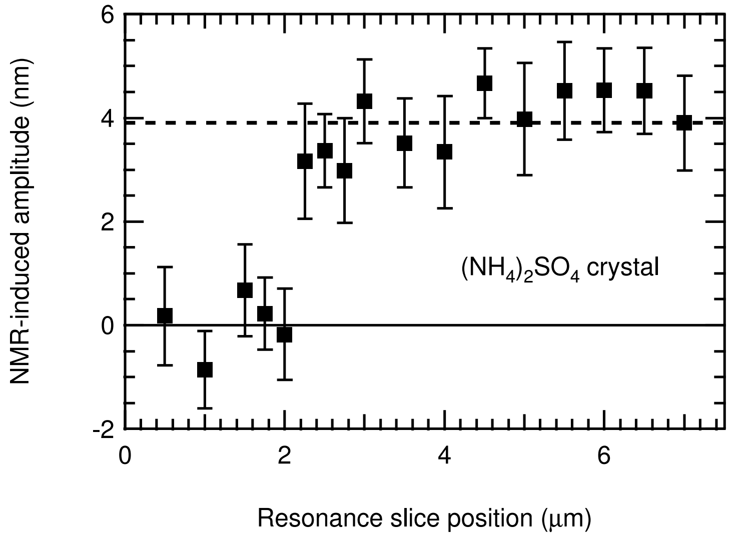

Figure 12. NMRFM force scan as a function of the resonant slice position for an ammonium sulfate crystal.

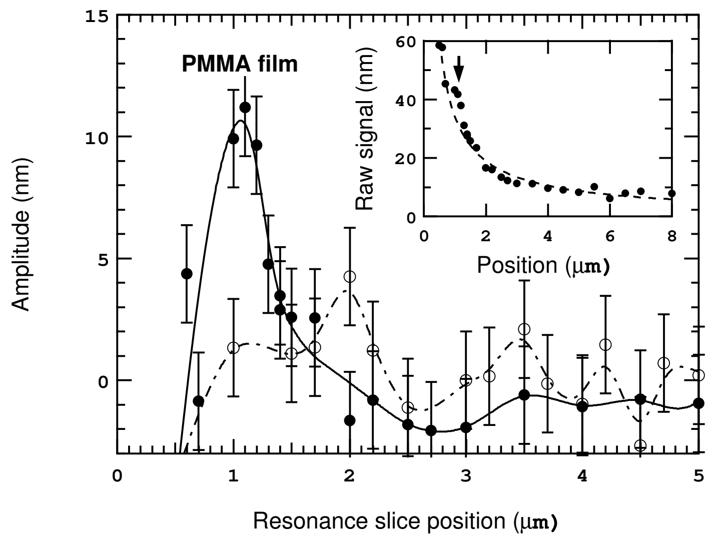

Figure 13. NMRFM force scan as a function of the resonant slice position for a PMMA thin film. The inset shows the force data, with an artifact that varies roughly inversely with resonant slice position z. The function $C_1 + C_2/z$ was subtracted from the data to obtain the portion of the signal that is nuclear magnetic in origin. The lines (spline fits) are guides to the eye.

We have recently fabricated micron-scale polymer islands for our planned three-dimensional scanning NMRFM experiments.

5. SUMMARY

We have microfabricated single-crystal-silicon mechanical oscillators using double-sided processing and characterized resonant frequencies, quality factors, spring constants, and force sensitivity. We then reported micromagnetometry, anisotropy, and dissipation studies of individual permalloy micromagnets on oscillators; the data can be understood within a single domain model. Using detailed modeling of the spatial dependence of the field and field gradient of our micromagnets, we were able to perform mechanical-oscillator detection of NMR in the magnet-on-oscillator scanning mode. We reported room-temperature detection of ^{1}H NMR in an ammonium-sulfate single-crystal with sensitivity of approximately 7×10^{-16} N and a very thin ($\sim$200 nm) resonant slice; we also detected ^{1}H NMR in a 0.3-μm-thick PMMA thin film with a force sensitivity of 2.0×10^{-16} N.

ACKNOWLEDGMENTS

This work was supported by the Army Research Office Contract No. DAAD-19-02-C-0064, the Robert A. Welch Foundation Grant No. F-1191, and the National Science Foundation under Grant Nos. DMR-0072365 and DMR-0210383.

REFERENCES

1. J. A. Sidles, J. L. Garbini, K. J. Brul, D. Rugar, O. Zűger, S. Hoen, and C. S. Yannoni, "Magnetic resonance force microscopy," *Rev. Mod. Phys.* **67**, pp. 249–265, 1995.
2. M. Chabot and J. Markert, "Microfabrication of single-crystal silicon multiple torsional oscillators," *Proc. SPIE* **3875**, pp. 104–112, 1999.
3. M. Chabot, T. Messina, V. Mancevski, C. Miller, and J. Markert, "Single-crystal silicon triple-torsional micro-oscillators for use in magnetic resonance force microscopy," *Proc. SPIE* **4559**, pp. 24–35, 2003.
4. M. Roukes, "Nanoelectromechanical systems face the future," *Physics World* **Feb.**, pp. 25–31, 2001.
5. R. N. Kleiman, G. K. Kaminsky, J. D. Reppy, R. Pindak, and D. J. Bishop, "Single-crystal silicon high-q torsional oscillators," *Rev. Sci.Instrum.* **56**, pp. 2088–2091, 1985.
6. A. L. Barr and J. Markert, "Fine structure in a high-resolution vortex dissipation study of $yba_2cu_3o_{7_\delta}$," *Phys. Rev. Lett.* **77**, pp. 731–734, 1996.
7. T. A. Barrett, C. R. Miers, H. A. Sommer, K. Mochizuki, and J. T. Markert, "Design and construction of a sensitive nuclear magnetic resonance force microscope," *J. Appl. Phys.* **83**, pp. 6235–6237, 1998.
8. K. Kim and S. Lee, "Self-oscillation mode induced in an atomic force microscope cantilever," *J. Appl. Phys.* **91**, pp. 4715–4719, 2002.
9. M. Zalalutdinov, A. Zehnder, A. Olkhovets, S. Turner, L. Sekaric, B. Ilic, D. Czaplewski, J. M. Parpia, and H. G. Craighead, "Autoparametric optical drive for micromechanical oscillators," *Appl. Phys. Lett.* **79**, pp. 695–697, 2001.
10. C. W. Miller, U. M. Mirsaidov, T. C. Messina, Y. J. Lee, and J. T. Markert, "External field effects on the resonant frequency of magnetically capped oscillators for magnetic resonance force microscopy," *J. Appl. Phys.* **93**, pp. 6572–6574, 2002.
11. B. C. Stipe, H. J. Mamin, T. D. Stowe, T. W. Kenny, and D. Rugar, "Magnetic dissipation and fluctuations in individual nanomagnets measured by ultrasensitive cantilever magnetometry," *Phys. Rev. Lett.* **86**, pp. 2874–2877, 2001.
12. D. Rugar, C. S. Yannoni, and J. A. Sidles, "Mechanical detection of magnetic resonance," *Nature* **360**, pp. 563–566, 1992.